Multifunctional TiO2-C/MnO2 Core-Double-Shell Nanowire Arrays as High-Performance 3D Electrodes for Lithium Ion Batteries

6 AUTHORS, INCLUDING:

Jin-Yun Liao
University of Texas at Austin
29 PUBLICATIONS   1,195 CITATIONS

SEE PROFILE

Drew C Higgins
University of Waterloo
70 PUBLICATIONS   2,089 CITATIONS

SEE PROFILE

Xingcheng Xiao
General Motors Company
177 PUBLICATIONS   2,638 CITATIONS

SEE PROFILE

Zhongwei Chen
University of Waterloo
179 PUBLICATIONS   5,233 CITATIONS

SEE PROFILE

Multifunctional TiO$_2$−C/MnO$_2$ Core−Double-Shell Nanowire Arrays as High-Performance 3D Electrodes for Lithium Ion Batteries

Jin-Yun Liao,[†] Drew Higgins,[†] Gregory Lui,[†] Victor Chabot,[†] Xingcheng Xiao,*[,‡] and Zhongwei Chen*[,†]

[†]Department of Chemical Engineering, Waterloo Institute for Nanotechnology, University of Waterloo, 200 University Avenue West, Waterloo, Ontario, Canada N2L 3G1

[‡]General Motors Global Research & Development Center, 30500 Mound Road, Warren, Michigan 48090, United States

S *Supporting Information*

ABSTRACT: The unique TiO$_2$−C/MnO$_2$ core−double-shell nanowires are synthesized for the first time using as anode materials for lithium ion batteries (LIBs). They combine both advantages from TiO$_2$ such as excellent cycle stability and MnO$_2$ with high capacity (1230 mA h g^{-1}). The additional C interlayer intends to improve the electrical conductivity. The self-supported nanowire arrays grown directly on current-collecting substrates greatly simplify the fabrication processing of electrodes without applying binder and conductive additives. Each nanowire is anchored to the current collector, leading to fast charge transfer. The unique one-dimensional core−double-shell nanowires exhibit enhanced electrochemical performance with a higher discharge/charge capacity, superior rate capability, and longer cycling lifetime.

KEYWORDS: Li-ion batteries, core−shell, TiO$_2$, MnO$_2$, nanowire, 3D
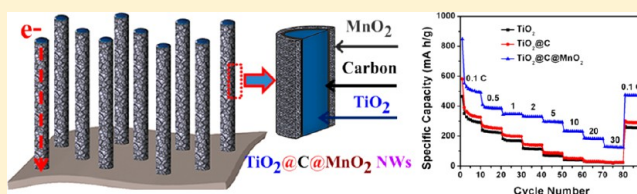
Due to their unique characteristics in terms of high energy density, long cycling life, and high operating voltage, rechargeable lithium ion batteries (LIBs) are widely considered to be one of the most promising choices available for the rapid development of mobile devices and electric vehicles.[1−8] Titanium dioxide (TiO$_2$) has attracted a lot of attention among the various transition metal oxides available for use as the active anode material in LIBs due to its attractive properties, including: (i) low cost, (ii) environmental friendliness, (iii) increased safety due to the higher Li-insertion potential (1.6− 1.8 V vs Li$^+$/Li) compared to commercialized carbon (graphite) anode materials, and (iv) low volume expansion during charge/discharge processes (3−4%) leading to long cycle life and durability. However, in practice the intrinsically slow transport kinetics for both electrons and Li ions in TiO$_2$ prevent optimal electrochemical performance.[9−11] Ongoing research activities are targeted toward techniques to improve the ionic and electronic transport properties of TiO$_2$, including carbon coating, ion doping, and nanostructure and morphology control.[12−15]

Recently, one-dimensional (1D) TiO$_2$ nanostructured materials such as nanowires, nanotubes, and nanorods have been investigated for LIBs.[16,17] Specifically, self-supported 1D nanostructures grown as ordered arrays directly on current collecting substrates are particularly interesting LIB materials owing to their vectorial ion and electron transport properties, and the ability to accommodate lithiation induced stresses.[18−20] Furthermore, the nanoscaled dimensions of these materials can also reduce the lithium ion diffusion lengths and, due to their large surface-to-volume ratio, can increase the lithium ion flux at the electrode/electrolyte interface. Unfortunately, in

comparison to conventional anode materials, TiO$_2$ has a relatively low theoretical capacity of around 335 mA h g^{-1}. Conversely, manganese dioxide (MnO$_2$) has attracted attention because of its high theoretical capacity of 1230 mA h g^{-1} and relatively low electrochemical motivation force.[21,22] MnO$_2$ has traditionally been used as a cathode material, but it has also been less frequently reported as an anode material for LIBs.[23−25] Nanostructured MnO$_2$ materials have been extensively developed, using various structures including nanowires, nanotubes, and nanoflakes to enhance anode performance in LIBs.[18,23−25] However, MnO$_2$ anodes suffer from rapid capacity fade during the cycling process due to volume expansion, aggregation, and intrinsically low electronic conductivity.

Methods involving layer-by-layer deposition have been widely used to fabricate core−shell nanoparticles and coaxial nanowires owing to the advantages of simplicity and thickness control at the nanoscale level.[26] Very recently, MnO$_2$ nanoparticles loaded onto a conductive layer using layer-by-layer deposition techniques have been reported to achieve high electrochemical performance for energy storage materials.[27−29] It was reported that MnO$_2$ nanoparticles could be grown onto a conductive polymer or a carbon layer by soaking the materials in potassium permanganate (KMnO$_4$) solution. The loading of MnO$_2$ nanoparticles over the conductive layer can enhance the capacity and stability of the nanocomposite material by introducing high capacity MnO$_2$ and providing a high active surface area. Three-dimensional ZnO−MnO$_2$ core−shell

nanostructures were also fabricated by the group of Mao et al. as supercapacitor electrode materials with highly improved specific capacitance.[30] Mai and co-workers recently reported cucumber-like V_2O_5/PEDOT and MnO_2 nanowires as cathode materials showing high Li^+ storage capacity and enhanced electrochemical cyclability in LIBs.[31] However, to the best of our knowledge no report using this methodology to fabricate MnO_2 based core−shell 1D nanostructured arrays as a 3D electrode has yet been applied to LIBs. Hence, it is highly desirable to design and synthesize a multifunctional core−shell 1D nanostructured electrode using layer-by-layer technique, which could simultaneously provide a high specific capacity, rate capability, and superior cyclability in LIBs.

In the present work we have designed and successfully synthesized TiO_2−C/MnO_2 core−double-shell nanowire arrays on flexible Ti foil. MnO_2 nanoparticles were produced on a TiO_2−C nanowire surface by combining the *in situ* chemical redox reaction between carbon and $KMnO_4$, using a facile soaking process. The unique core−double-shell nanowires obtained effectively couple the electrochemical functionality of the individual components including: the excellent stability of TiO_2, the excellent capacity of MnO_2, and the high electronic conductivity of the graphitic carbon layer. Specifically, the electrochemical Li ion insertion/extraction properties of the 3D anodes from TiO_2−C/MnO_2 core−double-shell nanowire arrays have been characterized, providing a gauge of their practical applicability toward LIBs. Notably, after MnO_2 nanoparticle loading, these unique core−double-shell 1D nanostructure array anodes demonstrated superior electrochemical performance including high charge/discharge capacities, excellent rate capabilities, and exemplary cycling performance.

The unique TiO_2−C/MnO_2 core−double-shell nanowire arrays on Ti-foil substrate were synthesized via a two-step layer-by-layer deposition growth process, and the preparation process is shown in Figure 1. It includes: (a, b) preparation of TiO_2 nanowires on Ti foil by alkali (NaOH) hydrothermal and ion exchange with HCl, followed by calcination; (c) carbon coating on TiO_2 nanowires via a glucose-assisted hydrothermal treatment, and subsequent heat treatment; and (d) MnO_2 nanoparticle decoration onto TiO_2−C nanowire arrays through immersion into $KMnO_4$ aqueous solution at room temperature (details shown in SEI). In these unique composite materials, the carbon coating provides dual functionality. First, it significantly enhances electron transport throughout the composite materials, and second, it facilitates the deposition of MnO_2 nanoparticles on the surface of TiO_2−C nanowire arrays via a redox reaction with the $KMnO_4$ solution (eq 1):[32]

$$4MnO_4^- + 3C + H_2O = 4MnO_2 + CO_3^{2-} + 2HCO_3^-$$

(1)
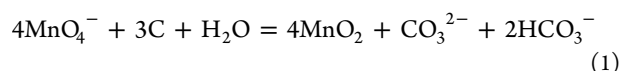
To determine the phase structure of the nanowire array products on titanium foils, XRD measurements were conducted on nanowire powder samples scraped off from the Ti substrates (Figure 2a). After the calcination process at 550 °C for 3 h, the $H_2Ti_2O_5$·H_2O was completely converted to anatase TiO_2 through a topotactic transformation,[33,34] and the TiO_2 nanowires can be indexed to the anatase structure phase (JCPDS No. 65-2900, a = 3.785, b = 3.785, c = 9.514).[33] The diffraction peaks of TiO_2−C core−shell nanowires after a carbon coating treatment have a consistent position with pure TiO_2 nanowires. The constant peak position indicates the phase structure of TiO_2 has not been changed through the carbon coating process. Furthermore, the carbon coating process did not provide any structural or morphological transformations as demonstrated by SEM and TEM results (Figures 3 and 4, respectively). Interestingly, after the second layer-by-layer deposition involving the deposition of MnO_2 nanoparticles, the XRD pattern of TiO_2−C/MnO_2 still only demonstrates the characteristic anatase TiO_2 phase. This is most likely due to the small amount of nanosized MnO_2 particles and the partially amorphous phase content being too low to show strong diffraction peaks.[27,31] The corresponding XRD patterns of nanowires on the Ti foil substrates were also conducted, and diffraction patterns are provided in the Supporting Information (Figure S1). Figure S1 reveals similar results to the diffraction peaks of the powder samples which are well-indexed to anatase TiO_2, with no noticeable diffraction peaks of MnO_2.

Raman spectra of the as-prepared nanowire products were measured to investigate the formation of the carbon layer and MnO_2 via the layer-by-layer deposition technique (Figure 2b). The observed peaks at 144, 400, 515, and 639 cm^{-1} for all three nanowires (TiO_2, TiO_2−C, and TiO_2−C/MnO_2) are characteristic of the anatase TiO_2 phase,[35] consistent with the results of XRD analysis. The TiO_2−C core−shell nanowires exhibit two additional peaks at ca. 1356 cm^{-1} and 1608 cm^{-1}, attributed to the D- and G-bands of carbon materials, respectively. This verifies the successful formation of a carbon coating, and the high intensity of the G-band compared to the D-band (I_D/I_G ratio of 0.27) indicates good graphitization of the carbon layer after treatment at 500 °C for 3 h in Ar. After MnO_2 loading, the TiO_2 peak located at 639 cm^{-1} was broadened to a range of 550−700 cm^{-1} due to overlapping MnO_2 peaks at around 530 cm^{-1} and 650 cm^{-1}. Two additional peaks were observed at ca. 630 and 575 cm^{-1}, which correspond to the symmetric stretching vibration (Mn−O) of the MnO_6 groups and the (Mn−O) stretching vibration in the basal plane of the MnO_6 sheets, respectively. Furthermore, the D- and G-bands of the
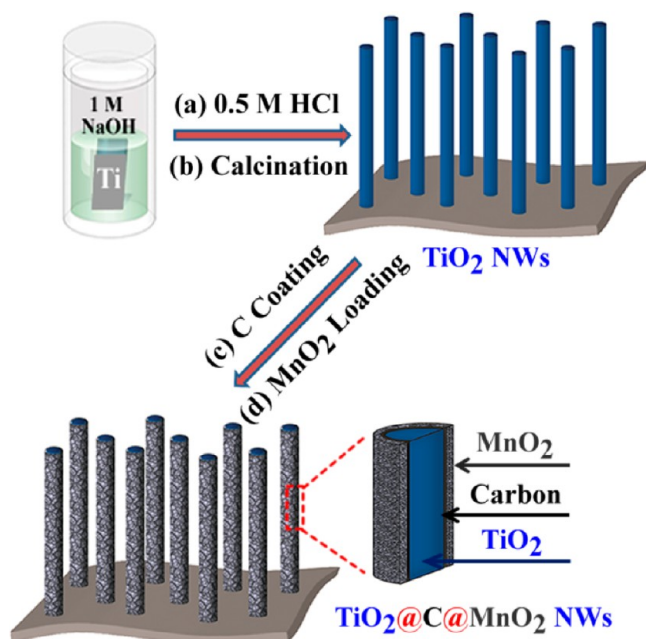

Figure 1. Schematic illustration for the fabrication of TiO_2−C/MnO_2 core−double-shell nanoiwre arrays on Ti foil.
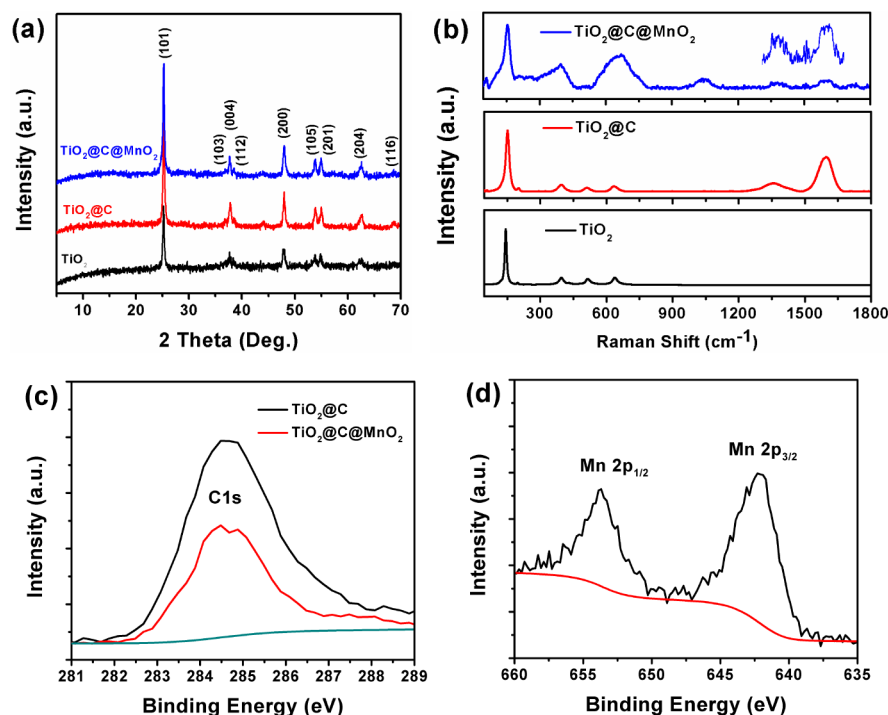
Figure 2. XRD patterns (a) and Raman spectra (b) of TiO_2, TiO_2-C, and TiO_2-C/MnO_2 nanowires; (c) XPS peaks of C1s of TiO_2-C and TiO_2-C/MnO_2 nanowires, and (d) XPS peaks of Mn2p of TiO_2-C/MnO_2 core−double-shell nanowires.

carbon materials were still present in the spectrum, indicating the successful synthesis of a three-layer composite material.

Figure 2c shows the C1s peak from XPS, which corresponds to the carbon layers in the TiO_2-C and TiO_2-C/MnO_2 nanowires. No obvious peaks are detected around 281.5 and 283 eV, indicating that the carbon was not doped into the TiO_2 lattice.[36] The characteristic C1s peak of TiO_2-C/MnO_2 has the same position as TiO_2-C, but shows decreased peak intensity. The intensity decrease can be explained by the formation of a layer of MnO_2 nanoparticles on the surface of TiO_2-C which reduced the amount of carbon due to the redox reaction with $KMnO_4$. The XPS spectra of TiO_2-C/MnO_2 (Figure 2d) show the peaks of $Mn2p_{3/2}$ and $Mn2p_{1/2}$ centered at 642.1 and 653.8 eV, respectively. The spin energy separation of 11.7 eV is in good agreement with reported data of $Mn2p_{3/2}$ and $Mn2p_{1/2}$ in MnO_2.[31] According to the full range XPS spectrum of TiO_2-C/MnO_2 nanowires shown in Figure S2a, the peak at around 293 eV shows the existence of K^+ in as-prepared core−double-shell nanostructures (Figure S2b), most likely arising due to formation of a residual byproducts (K_2CO_3 and/or $KHCO_3$) during the redox deposition of MnO_2.

Scanning electron microscopy (SEM) images of the as-prepared samples are shown in Figure 3, depicting the longitudinally enlarged SEM images of the TiO_2 (Figure 3a), TiO_2-C (Figure 3b), and TiO_2-C/MnO_2 (Figure 3c and d) nanowire arrays. The mean diameter and length of the as-prepared nanowires determined from SEM are 80 ± 5 nm and 12 ± 1 μm, respectively. After the carbon-coating process, the morphology of TiO_2-C nanowires (Figure 3b) remained unchanged in comparison to pure TiO_2 nanowires (Figure 3a), maintaining a smooth surface despite the hydrothermal and heat treatment. Immersing the TiO_2-C nanowires in an aqueous solution containing 0.03 M $KMnO_4$ initiated a redox reaction, which after 18 h led to the formation of sparse MnO_2 nanoparticles on the surface of the wires (Figure 3c). The
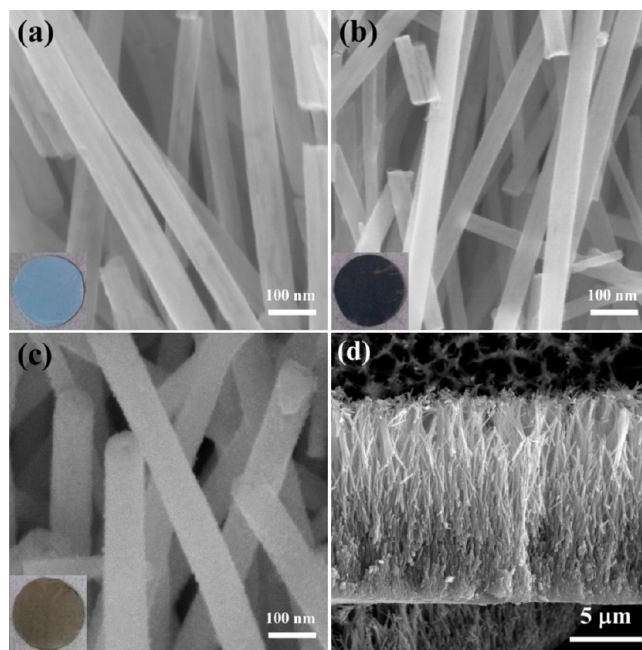

Figure 3. Cross-sectional SEM images of TiO_2 (a), TiO_2-C (b), and TiO_2-C/MnO_2 nanowires (c,d). Inset: photographs of the nanowire array film on Ti foil from different reaction steps.

different steps of layer formation can also be demonstrated by the changing color of the nanowire films (inset), which range from white (TiO_2) to black (TiO_2-C), and then to brown (TiO_2-C/MnO_2).

Further morphological and structural characterizations of the TiO_2, TiO_2-C, and TiO_2-C/MnO_2 nanowires were performed using TEM. High-resolution TEM (HRTEM) images of the prepared samples prepared at different steps are shown in Figure 4a−c. It is apparent that all prepared nanowire
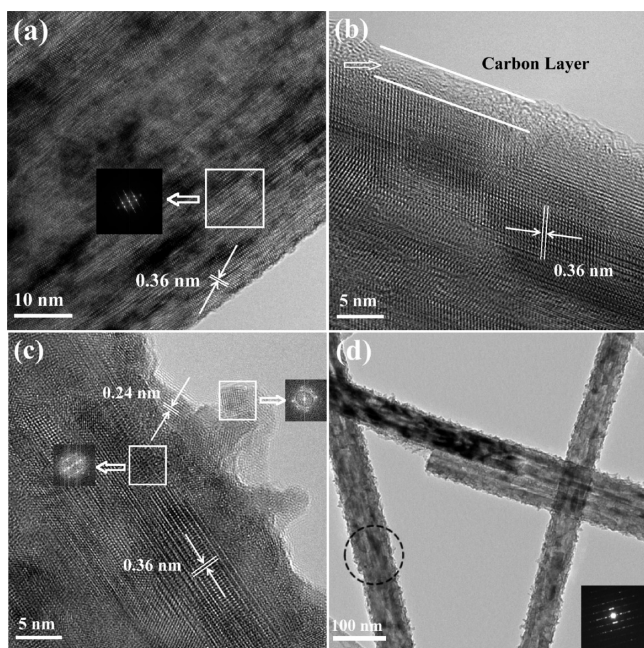
Figure 4. TEM images and FFT and SAED patterns (inset) of TiO_2 nanowire (a), TiO_2-C core−shell nanowire (b), and anatase TiO_2-C/MnO_2 core−double-shell nanowires (c, d).

Figure 5. EDS mapping of Ti (a), O (b), Mn (c), and C (d) from TiO_2-C/MnO_2 core−double-shell nanowire.

samples possess a single crystalline structure according to the selected area electron diffraction (SAED; Figure S3) and fast Fourier transform (FFT) patterns (inset of Figure 4). The single crystalline 1D structure can significantly increase the capabilities of electron and lithium ion diffusion in Li-ion batteries.[20,37] The measured interplanar spacing of 0.36 nm is in excellent agreement with the *d*-spacing of the anatase (101) planes. Figure 4a and Figure S3a show the typical as-prepared TiO_2 nanowire with a diameter of around 81 nm. The HRTEM of TiO_2-C shown in Figure 4b clearly displays the lattice fringes of anatase TiO_2, indicating preservation of the highly crystalline nature for the as-prepared TiO_2-C nanowires. Furthermore, the coated carbon layer has a uniform thickness of ca. 4 nm, creating a smooth, highly conductive layer over the entire nanowire surface. Compared with TiO_2-C nanowires (Figure 4b and Figure S3b), the TiO_2-C/MnO_2 nanowires (Figure 4c and d) have a rougher surface due to the MnO_2 nanoparticle formation, thereby improving the surface area of the active materials. The MnO_2 nanoparticles on TiO_2-C/MnO_2 nanowires are finely dispersed on the surface with a diameter of ca. 3−5 nm. While XRD analysis indicated that the MnO_2 nanoparticles are amorphous, HRTEM suggests the nanoparticles have a somewhat crystalline nature. An interplanar spacing of 0.24 nm was measured and relates to the *d*-spacing of MnO_2 (100) planes. It is therefore hypothesized that the absence of crystalline MnO_2 peaks from the XRD patterns is most likely due to the relatively small crystallite sizes (ca. 3 nm) in comparison with the sizing of the crystalline TiO_2 nanowires.

Energy-dispersive X-ray spectrometry (EDS) mapping analysis is shown in Figure 5 for a single hybrid nanowire, unambiguously confirming the structure of the TiO_2-C/MnO_2 core−double-shell. The distribution of C and Mn elements clearly encase the location of the Ti elements, which indicates that C and Mn distribute uniformly on the surface of the TiO_2 nanowire. The uniform elemental distribution and core−shell
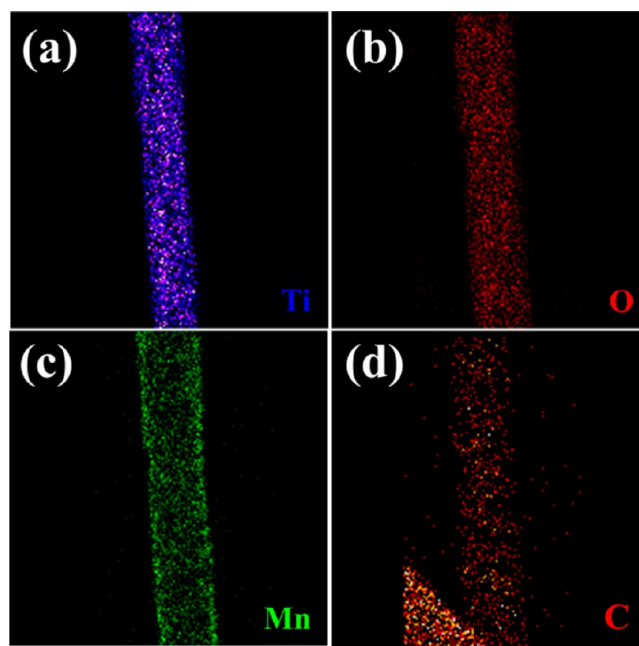
structure were further proven using EDS line scan spectra shown in Figure S4.

The electrochemical performance of the as-prepared TiO_2, TiO_2-C, and TiO_2-C/MnO_2 anodes were evaluated in half-cells utilizing metallic lithium film as the counter electrode and reference electrode. Figure 6a−c shows the cyclic voltammo-gram (CV) curves for TiO_2, TiO_2-C, and TiO_2-C/MnO_2 nanowire electrodes between 0.01 and 3 V (vs Li/Li^+) with a scan rate of 0.1 mV/s. The CV profile of the TiO_2 and TiO_2-C nanowire electrodes show three pairs of peaks, whereby the two pairs of cathodic/anodic peaks at 1.7−1.5 V were contributed by the TiO_2-B crystal phase,[12] and the other pair of cathodic/anodic peaks at around 2.1/1.7 V was contributed by anatase TiO_2. For the TiO_2-C/MnO_2 electrode, the main cathodic peak at around 2.5 V corresponds to electrolyte decom-position.[38] The main peak at around 0.5 V is assigned to the formation of a solid electrolyte interface (SEI) layer and the reduction of MnO_2, which is described by $MnO_2 + 4Li^+ + 4e^- \rightarrow Mn(0) + 2Li_2O$. Two more oxidation peaks at 1.25 and 2.1 V can also be observed, which means that the electrochemical oxidation reaction for MnO_2 may proceed by two steps.[38,39]

The initial three charge−discharge cycle profiles for the prepared TiO_2-based nanowire electrodes with a current rate of 0.1 C are shown in Figure 6d−f. The initial discharge capacities were 436 mA h g^{-1} for TiO_2, 576 mA h g^{-1} for TiO_2-C, to 865 mA h g^{-1} for the TiO_2-C/MnO_2 electrodes. The initial discharge capacities increased due to the capacity contribution of carbon for TiO_2-C and the presence of MnO_2 for TiO_2-C/MnO_2 nanowires. The stability was also enhanced by the carbon and MnO_2 layers, indicating this deposition method is an effective technique to simultaneously improve the electro-chemical specific capacity, cycle performance, and stability of nanowire electrodes in rechargeable LIBs. Flat discharge plateaus at around 1.7 and 1.5 V are observed in all three electrodes due to the Li ions being extracted from the anatase TiO_2 and TiO_2-B crystal phase, respectively, consistent with the anodic peak potentials observed by CV. The large first cycle
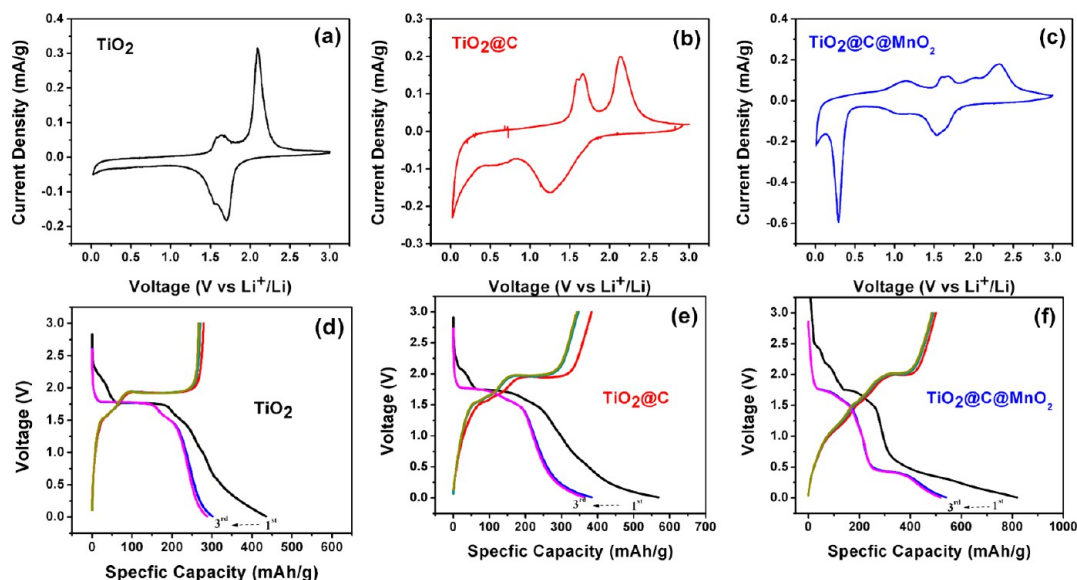
Figure 6. CV curves of TiO_2 (a), TiO_2-C (b), and TiO_2-C/MnO_2 nanowire (d) electrodes at a scan rate of 0.1 mV s^{-1} between 0.01 and 3 V and the first three charge−discharge curves at 0.1 C of TiO_2 (d), TiO_2-C (e), and TiO_2-C/MnO_2 nanowire (f) electrodes.
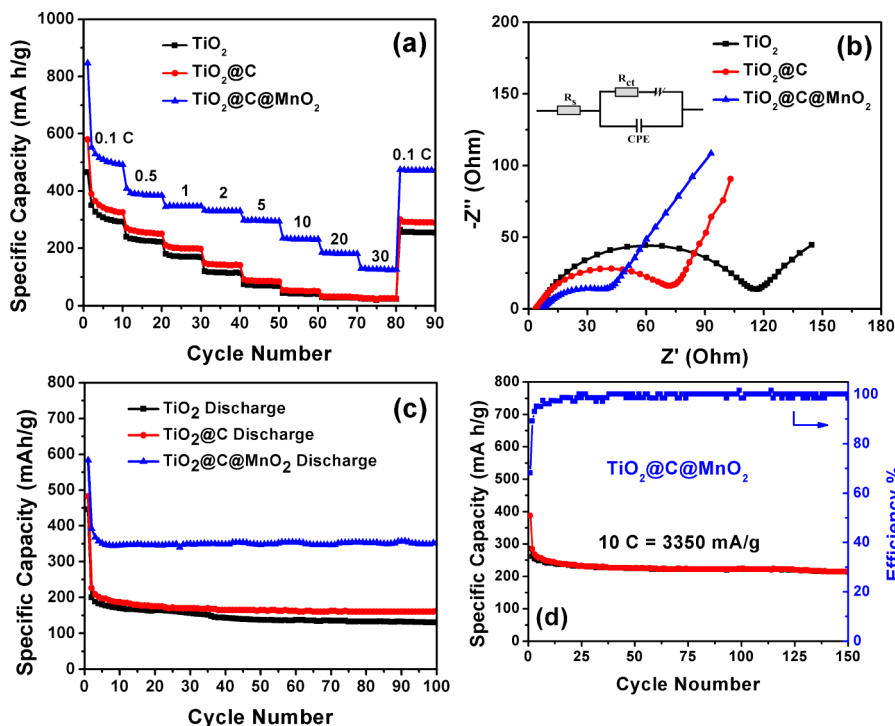

Figure 7. Electrochemical properties of TiO_2, TiO_2-C, and TiO_2-C/MnO_2 nanowire electrodes. (a) The rate performance at various current densities from 0.1 to 30 C (1 C = 335 mA/g); (b) electrochemical impedance spectra (Nyquist plots) of electrodes at full charge states; (c) cyclic performance of the two electrodes beyond 100 cycles at a rate of 1 C and (d) at 10 C up to 150 cycles for TiO_2-C/MnO_2 electrode between 0.01 and 3 V (vs Li/Li$^+$).
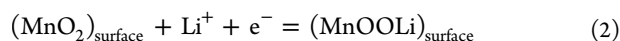
capacity loss of the TiO_2-C/MnO_2 core−double-shell electrodes, shown in Figure 6f, was caused by: (i) irreversible intercalation of Li ions with TiO_2, (ii) irreversible conversion of MnO_2 by Li ions, and (iii) the formations of a solid−electrolyte interface (SEI) layer on MnO_2 by electrolyte decomposition. The voltage plateau and anodic peak from CV testing (Figure 6c) around 0.4 V verified the conversion reactions of MnO_2 nanoparticles to Mn metal with Li_2O formation, which is commonly observed for a variety of transition-metal oxide electrode materials.[40,41]

Rate capability is another very important consideration for practical Li-ion batteries. To examine the effect of the carbon and MnO_2 layers on rate capability, these three TiO_2 nanowire based electrodes were studied by charging/discharging at different C rates ranging from 0.1 to 30 C (1 C = 335 mA/ g). As shown in Figure 7a, the TiO_2-C electrode exhibits a higher capacity and improved rate performance, with discharge capacities of 258, 145, and 56 mA h g^{-1} at 0.5, 2, and 10 C, respectively. Meanwhile, the pure TiO_2 nanowire electrode only maintained discharge capacities of 225, 112, and 38 mA h

g^{-1} at 0.5, 2, and 10 C, respectively. The improved performance is most likely due to the superior electronic conductivity for the carbon coated TiO_2–C nanowire electrode. Upon comparison of the TiO_2–C and TiO_2–C/MnO_2 electrodes at different discharge rates, the TiO_2–C/MnO_2 core–double-shell electrode shows superior performance, with discharge capacities of 332, 298, 235, 186, and 130 mA h g^{-1} at 2, 5, 10, 20, and 30 C, respectively. In contrast, the TiO_2–C electrode only maintained discharge capacities of 33 and 24 mA h g^{-1} at high rates of 20 and 30 C, respectively. This enhanced rate performance could be due to the: (i) unique one-dimensional core–double-shell structure provides fast Li ion transportation throughout the electrode, (ii) high electronic conductivity of the carbon layer, and (iii) high capacity of the MnO_2 active materials. After measuring high rate capacity, the TiO_2–C/MnO_2 anode is still able to provide capacity of 471 mA h g^{-1} at 0.1 C, corresponding to initial capacity retention of 93%. This exclusively demonstrates the improved rate stability of these materials over the TiO_2 nanowire (85% capacity retention) and TiO_2–C core–shell nanowire anode (90% capacity retention).

To understand the enhanced rate capability, resistance was analyzed by electrochemical impedance spectroscopy (EIS). Nyquist plots of the three TiO_2 nanowire based electrodes are shown in Figure 7b. The Nyquist plots of all three electrodes depict a semicircle at high-medium frequency and an inclined line at low frequency, which correspond to charge transfer and diffusion, respectively. The components of the equivalent circuit (inset in Figure 7b) include: R_s as the ohmic resistance (total resistance of the electrolyte, separator, and electrical contacts), R_{ct} as the charge transfer resistance, W as the Warburg impedance of Li ion diffusion into the active materials, and CPE is the constant phase-angle element which involves the double layer capacitance. The transfer resistances (R_{ct}) of TiO_2, TiO_2–C, and TiO_2–C/MnO_2 nanowire electrodes are 120.6, 82.1, and 49.2 ohm, respectively. This suggests that the TiO_2–C/MnO_2 nanowire arrays have the lowest activation energy for the Li^+ diffusion and undergo a fast Faradaic reaction, which supports the increased high-rate performance of the TiO_2–C/MnO_2 anode in comparison to the other two electrodes.

Figure 7c compares the cycling performance of these three nanowire electrodes at 1C in the voltage range of 0.01–3 V. The discharge capacities of TiO_2, TiO_2–C, and TiO_2–C/MnO_2 nanowire electrodes after 100 cycles are 130, 162, and 352 mA h g^{-1}, showing 65%, 71%, and 90% retention of second discharge capacity, respectively. The higher capacity retention for TiO_2–C electrodes can be ascribed to the presence of the carbon layer on the surface of the TiO_2 nanowires, providing mechanical protection and stabilizing the SEI layer at lower potential. The higher capacity retention of TiO_2–C/MnO_2 nanowires is owing to the larger specific surface and high theoretical capacity of MnO_2. Specifically, MnO_2 nanoparticles can adsorb Li cations from the electrolyte according to eq 2:[31]

$$(MnO_2)_{surface} + Li^+ + e^- = (MnOOLi)_{surface} \qquad (2)$$

Thus, they contribute particular Li^+ intercalation and deintercalation capabilities.[26,42] Moreover, after operating the TiO_2–C/MnO_2 core–double-shell nanowire electrode at 10 C for 150 cycles the discharge capacity was 218 mA h g^{-1}, with a high Coulombic efficiency of around 99.9% (Figure 7d). The significant improvements in specific capacity and rate performance for the TiO_2–C/MnO_2 core–double-shell nanowires, compared to the other two nanowire electrodes, are mainly

attributed to fast electron/ion transportation along the 1D TiO_2 nanowires, the enhanced electrical conductivity carbon, and the considerable enhancement to surface charge transfer (Figure 7b).

In summary, single crystalline TiO_2, TiO_2–C, and TiO_2–C/MnO_2 nanowire arrays were successfully fabricated on flexible Ti substrates through a layer-by-layer deposition technique, and their electrochemical characteristics were investigated for use in LIBs. The TiO_2–C core–shell nanowires were first obtained via a hydrothermal carbon coating method. Then, by simply soaking the electrodes in aqueous $KMnO_4$ solution an *in situ* redox reaction occurred, forming the final TiO_2–C/MnO_2 core–double-shell nanowires. The electrochemical performance investigation of the self-supported, additive free anode materials, revealed that the unique TiO_2–C/MnO_2 core–double-shell nanowires exhibited enhanced electrochemical cycling and rate properties compared to that of the TiO_2 and TiO_2–C nanowires. Specifically, the TiO_2–C/MnO_2 core–double-shell nanowire electrodes showed a high charge/discharge capacity and excellent rate performance of 332, 298, 235, 186, and 130 mA h g^{-1} at 2, 5, 10, 20, and 30 C (1 C = 335 mA/g), respectively. This highly improved electrochemical performance is ascribed to the stable structure of the TiO_2 nanowire core, high conductivity of the carbon layer, higher active surface area, and high theoretical capacity of MnO_2. This work illustrates that the layer-by-layer method is an effective technique for preparing unique single crystalline TiO_2–C/MnO_2 nanowire arrays and that these arrays are very promising high rate anode materials for advanced carbon black and binder free LIB applications.

■ ASSOCIATED CONTENT

Ⓢ Supporting Information
Experimental details and materials characterizations including XRD patterns of nanowires on Ti foil, TEM images of TiO_2 and TiO_2–C nanowires, XPS of TiO_2–C/MnO_2 nanowires, and EDS line scan images of TiO_2–C/MnO_2 nanowires. This material is available free of charge via the Internet at http://pubs.acs.org.

■ AUTHOR INFORMATION

Corresponding Authors
*E-mail: zhwchen@uwaterloo.ca.
*E-mail: xingcheng.xiao@gm.com.
Notes
The authors declare no competing financial interest.

■ ACKNOWLEDGMENTS

■ REFERENCES

(1) Tarascon, J. M.; Armand, M. *Nature* **2001**, *414* (6861), 359–367.
(2) Sun, Y. K.; Myung, S. T.; Park, B. C.; Prakash, J.; Belharouak, I.; Amine, K. *Nat. Mater.* **2009**, *8* (4), 320–324.
(3) Wang, F.; Robert, R.; Chernova, N. A.; Pereira, N.; Omenya, F.; Badway, F.; Hua, X.; Ruotolo, M.; Zhang, R. G.; Wu, L. J.; Volkov, V.;

Su, D.; Key, B.; Whittingharn, M. S.; Grey, C. P.; Amatucci, G. G.; Zhu, Y. M.; Graetz, J. *J. Am. Chem. Soc.* **2011**, *133* (46), 18828−18836.

(4) Bruce, P. G.; Scrosati, B.; Tarascon, J. M. *Angew. Chem., Int. Ed.* **2008**, *47* (16), 2930−2946.

(5) Hassan, F. M.; Chen, Z. W.; Yu, A. P.; Chen, Z.; Xiao, X. C. *Electrochim. Acta* **2013**, *87*, 844−852.

(6) Ahn, D.; Xiao, X. C.; Li, Y. W.; Sachdev, A. K.; Park, H. W.; Yu, A. P.; Chen, Z. W. *J. Power Sources* **2012**, *212*, 66−72.

(7) Lee, H. W.; Muralidharan, P.; Ruffo, R.; Mari, C. M.; Cui, Y.; Kim, D. K. *Nano Lett.* **2010**, *10* (10), 3852−3856.

(8) Liu, N.; Wu, H.; McDowell, M. T.; Yao, Y.; Wang, C. M.; Cui, Y. *Nano Lett.* **2012**, *12* (6), 3315−3321.

(9) Wang, D. H.; Choi, D. W.; Li, J.; Yang, Z. G.; Nie, Z. M.; Kou, R.; Hu, D. H.; Wang, C. M.; Saraf, L. V.; Zhang, J. G.; Aksay, I. A.; Liu, J. *ACS Nano* **2009**, *3* (4), 907−914.

(10) Hu, Y. S.; Kienle, L.; Guo, Y. G.; Maier, J. *Adv. Mater.* **2006**, *18* (11), 1421−1426.

(11) Wagemaker, M.; Kentgens, A. P. M.; Mulder, F. M. *Nature* **2002**, *418* (6896), 397−399.

(12) Wang, Y.; Su, X. W.; Lu, S. *J. Mater. Chem.* **2012**, *22* (5), 1969−1976.

(13) Ren, Y.; Liu, Z.; Pourpoint, F.; Armstrong, A. R.; Grey, C. P.; Bruce, P. G. *Angew. Chem., Int. Ed.* **2012**, *51* (9), 2164−2167.

(14) Peng, Z. Y.; Shi, Z.; Liu, M. L. *Chem. Commun.* **2000**, *21*, 2125−2126.

(15) Liao, J. Y.; Xiao, X. C.; Higgins, D.; Lee, D.; Hassan, F.; Chen, Z. W. *Electrochim. Acta* **2013**, *108* (1), 104−111.

(16) Li, J. M.; Wan, W.; Zhou, H. H.; Li, J. J.; Xu, D. S. *Chem. Commun.* **2011**, *47* (12), 3439−3441.

(17) Brutti, S.; Gentili, V.; Menard, H.; Scrosati, B.; Bruce, P. G. *Adv. Energy Mater.* **2012**, *2* (3), 322−327.

(18) Xiong, H.; Slater, M. D.; Balasubramanian, M.; Johnson, C. S.; Rajh, T. *J. Phys. Chem. Lett.* **2011**, *2* (20), 2560−2565.

(19) Wang, L. L.; Wu, X. M.; Zhang, S. C. *Mech. Electron. Eng. III, Pts 1−5* **2012**, *130−134*, 1281−1285.

(20) Liu, B.; Deng, D.; Lee, J. Y.; Aydil, E. S. *J. Mater. Res.* **2010**, *25* (8), 1588−1594.

(21) Yu, A. P.; Park, H. W.; Davies, A.; Higgins, D. C.; Chen, Z. W.; Xiao, X. C. *J. Phys. Chem. Lett.* **2011**, *2* (15), 1855−1860.

(22) Wu, M. S.; Chiang, P. C. J.; Lee, J. T.; Lin, J. C. *J. Phys. Chem. B* **2005**, *109* (49), 23279−23284.

(23) Sayle, T. X. T.; Maphanga, R. R.; Ngoepe, P. E.; Sayle, D. C. *J. Am. Chem. Soc.* **2009**, *131* (17), 6161−6173.

(24) Su, D.; Ahn, H. J.; Wang, G. *J. Mater. Chem. A* **2013**, *1* (15), 4845−4850.

(25) Jiao, F.; Bruce, P. G. *Adv. Mater.* **2007**, *19* (5), 657−660.

(26) Luo, W.; Hu, X. L.; Sun, Y. M.; Huang, Y. H. *J. Mater. Chem.* **2012**, *22* (11), 4910−4915.

(27) Liu, R.; Lee, S. B. *J. Am. Chem. Soc.* **2008**, *130* (10), 2942−2943.

(28) Liu, R.; Duay, J.; Lee, S. B. *ACS Nano* **2010**, *4* (7), 4299−4307.

(29) Yu, G. H.; Hu, L. B.; Liu, N. A.; Wang, H. L.; Vosgueritchian, M.; Yang, Y.; Cui, Y.; Bao, Z. A. *Nano Lett.* **2011**, *11* (10), 4438−4442.

(30) Sun, X.; Li, Q.; Lu, Y.; Mao, Y. *Chem. Commun.* **2013**, *49* (40), 4456−4458.

(31) Mai, L. Q.; Dong, F.; Xu, X.; Luo, Y. Z.; An, Q. Y.; Zhao, Y. L.; Pan, J.; Yang, J. N. *Nano Lett.* **2013**, *13* (2), 740−745.

(32) Fan, Z. J.; Yan, J.; Wei, T.; Zhi, L. J.; Ning, G. Q.; Li, T. Y.; Wei, F. *Adv. Funct. Mater.* **2011**, *21* (12), 2366−2375.

(33) Liao, J. Y.; Lei, B. X.; Chen, H. Y.; Kuang, D. B.; Su, C. Y. *Energy Environ. Sci.* **2012**, *5* (2), 5750−5757.

(34) Liu, B.; Boercker, J. E.; Aydil, E. S. *Nanotechnology* **2008**, *19* (50), 505604.

(35) Chen, X. B.; Liu, L.; Yu, P. Y.; Mao, S. S. *Science* **2011**, *331* (6018), 746−750.

(36) Jia, F. Z.; Yao, Z. P.; Jiang, Z. H.; Li, C. X. *Catal. Commun.* **2011**, *12* (6), 497−501.

(37) Foll, H.; Hartz, H.; Ossei-Wusu, E.; Carstensen, J.; Riemenschneider, O. *Phys. Status. Solidi-R* **2010**, *4* (1−2), 4−6.

(38) Xia, H.; Lai, M. O.; Lu, L. *J. Mater. Chem.* **2010**, *20* (33), 6896−6902.

(39) Lai, H.; Li, J. X.; Chen, Z. G.; Huang, Z. G. *ACS Appl. Mater. Interfaces* **2012**, *4* (5), 2325−2328.

(40) Ko, Y. D.; Kang, J. G.; Park, J. G.; Lee, S.; Kim, D. W. *Nanotechnology* **2009**, *20* (45), 455701.

(41) Li, Y. G.; Tan, B.; Wu, Y. Y. *Nano Lett.* **2008**, *8* (1), 265−270.

(42) Reddy, A. L. M.; Shaijumon, M. M.; Gowda, S. R.; Ajayan, P. M. *Nano Lett.* **2009**, *9* (3), 1002−1006.